11th ANKARA INTERNATIONAL AEROSPACE CONFERENCE **AIAC-2021-160**
8-10 September 2021 - METU, Ankara TURKEY

INITIAL DATA COMPATIBILITY CHECK EFFORT FOR T625 FLIGHT DATA

Yusuf Onur Arslan[1] and Ilgaz Doğa Okcu[2]
TUSAŞ
Ankara, TURKEY

ABSTRACT

A data consistency method for a medium weight utility helicopter flight test program is being developed by flight mechanics group in Turkish Aerospace. The primary aim of this method is to aid flight mechanics and autopilot design for T625 helicopter during flight testing phase. This paper summarizes the initial progress on data compatibility analysis. Primary method for compatibility check is chosen as the Kalman Filter so that noise can be removed from data when the data is available as a measurement, and data can be estimated or observed when it is not directly measured by the flight test instrumentation suit. This work presents the general procedure for data process, with some selected analysis cases.

INTRODUCTION

A detailed and correct set of flight test data is necessary for model validation and system identification studies of an aircraft. In reality; however, the flight test data almost always have systematic and/or random measurement errors. Data consistency check should be performed in order to evaluate the quality of the data and the detected errors must be removed. A comprehensive data consistency check procedure is often disregarded by the analyst, despite being a vital step before flight data analysis. Consistent flight data could very well determine the success or failure of any given analysis method. Moreover, inconsistent data can lead to faulty evaluations about the flight characteristics of an aircraft which possesses a huge risk in terms of flight safety and cost especially for new development programs.

Consistency check is a natural extension of first principles based mathematical modeling. Translational dynamic and rotational kinematic equations provide a credible mathematical model basis for analysis. In cases where the model equations are as reliable as 6 DoF relations, Kalman Filter algorithm provides a powerful way of filtering and/or observing the required data. Although several reliable methods exist for consistency check like the maximum likelihood estimator or least squares, this work utilizes Kalman Filter approach due to its online estimation ability [Evans et al., 1985].

A simple and valid mathematical model is the key for the approach described in this paper. A valid mathematical model more or less eliminates the errors due to modeling uncertainty. Then, inconsistencies in the measurement data can be explained by the measurement errors. Bias,

[1] Design Eng. in Flight Mechanics and Autopilot Department, Email: yusufonur.arslan@tai.com.tr

[2] Design Eng. in Flight Mechanics and Autopilot Department, Email: iokcu@tai.com.tr

scale factor, time shift and drift are classified as systematic errors and they can arise from a couple of reasons. These reasons include but are not limited to axes misalignment, location offset and asynchronous sampling. On the other hand, drop out, disturbance and quantization errors are classified as random errors and they can originate from loss of telemetry, interference with outsources or sensor resolution [Tischler and Remplr, 2006].

The studies of state estimation of an aircraft goes back in 70's [Wingrove, 1972] [Klein and Schiess, 1977]. NASA developed a generic state estimation program, called SMACK, based on Wingrove's work [Bach, 1991]. It is useful for estimating wind and correcting sensor measurements. SMACK is utilized in order to examine and correct data consistency errors in a flight test data of the Bo-105 helicopter [Fletcher, 1990]. The state estimation is not limited to aircraft itself, but also it can include human-pilot model parameters [Schiess and Rolan, 1975] or maneuvers of a missile target [Tang and Borrie, 1984]. Furthermore, state estimation usage dramatically increased in robotics applications [Xiong and Chu, 2006] [Nasir et al., 2017] and spacecraft studies [Soken and Sakai, 2015] [Abreu, Oliveira and Neto, 2020].

In this study, the data compatibility check is performed by using the Kalman Filter for T625 helicopter flight test data using the minimum set of state variables for dynamic and kinematic equations. First, main rotor azimuth measurement consistency is checked using linear Kalman Filter for driveshaft rotational kinematics and dynamics. Input prediction capability of Kalman Filter is also demonstrated using the same rotational shaft kinematic model. Then, the data compatibility check is performed for the helicopter using extended Kalman Filter for the rigid body dynamics equations of motion. Additionally, wind speed is estimated based on the rigid body equations of motion in body-fixed coordinate system, demonstrating the Kalman Filter's observation capabilities.

METHOD

Mathematical Models

Kalman Filter is an optimal estimator under the least-squares assumption [Thrun, Burgard and Fox, 2005]. It is essentially a specialized Bayes Filter algorithm for unimodal probability distributions. Kalman Filter requires a mathematical model for predicting the states, and measurement model for correcting the state estimates. A process noise covariance matrix and a measurement noise covariance matrix are used to weigh the trustworthiness of prediction and measurement updates.

The main idea behind this work is to use simple and dependable prediction models with low process noise covariance in order to effectively estimate and eliminate measurement errors. Following analysis cases use two different simple dynamic/kinematic prediction update models. First model is the driveshaft dynamics and the second model is the 6 DoF translational dynamics and rotational kinematics of a rigid body in space. Accompanying measurement models for both models are also presented in this chapter for the sake of completeness.

The driveshaft dynamics of the main rotor fits the requirements of this paper in terms of its simplicity and accountability. A Taylor Series Expansion of the main rotor shaft position results in the dynamic relations. If the expansion is used up to the third term, position-velocity-acceleration relation can be easily put forward as a linear first order differential equation set.

$$\begin{aligned} \boldsymbol{\psi_{t+1}} &= \boldsymbol{\psi_t} + \dot{\boldsymbol{\psi}}_t \boldsymbol{\Delta t} + \ddot{\boldsymbol{\psi}}_t \frac{\boldsymbol{\Delta t^2}}{\boldsymbol{2}} \\ \dot{\boldsymbol{\psi}}_{\boldsymbol{t+1}} &= \dot{\boldsymbol{\psi}}_t + \ddot{\boldsymbol{\psi}}_t \boldsymbol{\Delta t} \end{aligned} \tag{1}$$

Measurement or observation equations for this case is both the angular position itself and angular velocity. Angular position is measured with the help of a tachometer (TAC) installed on helicopter main rotor shaft and the angular velocity measurement comes from the Engine Control Unit (ECU). Moreover, tachometer provides angular velocity data too. Thus, all states are measured and measurement equations for state variables are just equalities. The input, state and measurement vectors for main rotor driveshaft dynamics is then;

$$\begin{aligned} \boldsymbol{u} &= \ddot{\boldsymbol{\psi}} \\ \boldsymbol{x} &= [\boldsymbol{\psi}\ \dot{\boldsymbol{\psi}}]^{\boldsymbol{T}} \\ \boldsymbol{z} &= [\boldsymbol{\psi}\ \dot{\boldsymbol{\psi}}]^{\boldsymbol{T}} \end{aligned} \tag{2}$$

Hence, the linear system is formed as;

$$\boldsymbol{A} = \begin{bmatrix} \mathbf{1} & \boldsymbol{dt} \\ \mathbf{0} & \mathbf{1} \end{bmatrix} \qquad \boldsymbol{B} = \begin{bmatrix} \frac{\boldsymbol{dt^2}}{\mathbf{2}} & \boldsymbol{dt} \end{bmatrix} \tag{3}$$

Beside state estimation, another usage of Kalman Filter is the input estimation. Actually, this is achieved by introducing the input as another state of the system. The state and the output matrices can be modified as in the reference [Verhaegen & Verdult, 2012];

$$\widehat{\boldsymbol{A}} = \begin{bmatrix} \boldsymbol{A} & \boldsymbol{B} \\ \mathbf{0} & \boldsymbol{I} \end{bmatrix} \qquad \widehat{\boldsymbol{C}} = [\boldsymbol{C} \quad \mathbf{0}] \tag{4}$$

And, augmented states becomes;

$$\widehat{\boldsymbol{x}} = [\boldsymbol{x}\ \boldsymbol{u}]^{\boldsymbol{T}} \tag{5}$$

The nonlinear system is represented in Equation 6. In this case, $\boldsymbol{u_m}$is the measured input vector, $\boldsymbol{w}$ is the noise in the input measurements, and $\boldsymbol{v}$ is the noise in the output measurements. Translational dynamics and rotational kinematics are adapted from the equations of motion of a helicopter given in reference [Jategaonkar, 2006].

$$\begin{aligned} \dot{\boldsymbol{x}}(\boldsymbol{t}) &= \boldsymbol{f}(\boldsymbol{x}(\boldsymbol{t}), \boldsymbol{u_m}(\boldsymbol{t}) - \boldsymbol{w}(\boldsymbol{t})) \\ \boldsymbol{y}(\boldsymbol{t}) &= \boldsymbol{g}(\boldsymbol{x}(\boldsymbol{t})) \\ \boldsymbol{z}(\boldsymbol{t_k}) &= \boldsymbol{y}(\boldsymbol{t_k}) + \boldsymbol{v}(\boldsymbol{t_k}) \end{aligned} \tag{6}$$

$$\begin{aligned} \dot{\boldsymbol{u}} &= -\boldsymbol{qw} + \boldsymbol{rv} - \boldsymbol{gsin\theta} + \boldsymbol{a_x} \\ \dot{\boldsymbol{v}} &= -\boldsymbol{ru} + \boldsymbol{pw} + \boldsymbol{gcos\theta sin\phi} + \boldsymbol{a_y} \\ \dot{\boldsymbol{w}} &= -\boldsymbol{pv} + \boldsymbol{qu} + \boldsymbol{gcos\theta cos\phi} + \boldsymbol{a_z} \\ \dot{\boldsymbol{\phi}} &= \boldsymbol{p} + \boldsymbol{qsin\phi tan\theta} + \boldsymbol{rcos\phi tan\theta} \\ \dot{\boldsymbol{\theta}} &= \boldsymbol{qcos\phi} - \boldsymbol{rsin\phi} \\ \dot{\boldsymbol{\psi}} &= \boldsymbol{qsin\phi sec\theta} + \boldsymbol{rcos\phi sec\theta} \end{aligned} \tag{7}$$

Equations 7 constitute the prediction model for a helicopter flight. Since the linear acceleration and the angular rate data are available as measurement, the state variables can be estimated using these relations. State variables are the body velocities, Euler angles and wind speed in body frame. Both body velocities and Euler angles are measured directly; thus, their measurement models are just equalities. However, the measurement update of wind states is made through the freestream measurements, which are indicated airspeed, angle of attack and angle of sideslip.
The inputs, states and measurements for the 6 DoF model used in this work can be summarized in Equation 8.

$$\begin{gathered} \boldsymbol{u} = \left[\boldsymbol{a_x}\ \boldsymbol{a_y}\ \boldsymbol{a_z}\ \boldsymbol{p}\ \boldsymbol{q}\ \boldsymbol{r}\ \boldsymbol{a_{x_{wind}}}\ \boldsymbol{a_{y_{wind}}}\ \boldsymbol{a_{z_{wind}}}\right]^{\boldsymbol{T}} \\ \boldsymbol{x} = [\boldsymbol{u}\ \boldsymbol{v}\ \boldsymbol{w}\ \boldsymbol{\phi}\ \boldsymbol{\theta}\ \boldsymbol{\psi}\ \boldsymbol{u_{wind}}\ \boldsymbol{v_{wind}}\ \boldsymbol{w_{wind}}]^{\boldsymbol{T}} \\ \boldsymbol{z} = [\boldsymbol{u}\ \boldsymbol{v}\ \boldsymbol{w}\ \boldsymbol{\phi}\ \boldsymbol{\theta}\ \boldsymbol{\psi}\ \boldsymbol{V}\ \boldsymbol{\alpha}\ \boldsymbol{\beta}]^{\boldsymbol{T}} \end{gathered} \tag{8}$$

Kalman Filter

Kalman Filter can be applied to linear and nonlinear systems. For nonlinear systems, the state and output equations are linearized around the point of interest and the algorithm proceeds as in the linear case. The Kalman Filter implementation for nonlinear systems is called extended Kalman Filter. In order not to create confusion, linear Kalman Filter method is abbreviated as KF and extended Kalman Filter is abbreviated as EKF. Since the driveshaft can be easily modelled as linear, in this case, KF usage is assessed as appropriate. On the other hand, 6 DoF equations of motion include nonlinearities and, therefore, EKF implementation is preferred.

Equation 9, shows the general prediction model form or the *prediction update* step used in KF. Equation 10 is defined as the *measurement update* step. $\boldsymbol{A_t}$ and $\boldsymbol{B_t}$ are the linear model state and input matrices corresponding to time **t**. $\overline{\boldsymbol{\mu_t}}$ represents the mean state prediction and $\boldsymbol{\mu_t}$ is the updated mean state prediction using measurements. $\boldsymbol{\Sigma}$ and $\overline{\boldsymbol{\Sigma}}$ represent the covariance of the state variables for prediction step and measurement update step. Note that, KF algorithm represents the *state belief* at any given instant as a mean vector and a covariance matrix since the unimodal probability distribution assumption for all the variables involved has been done beforehand. $\boldsymbol{z_t}$ is measurement vector and $\boldsymbol{K_t}$ is the Kalman gain. KF algorithm updates both mean and covariance prediction at every step, resulting in a state belief in a stochastic framework.

$$\begin{gathered} \overline{\boldsymbol{\mu}}_{\boldsymbol{t}} = \boldsymbol{A_t}\boldsymbol{\mu_{t-1}} + \boldsymbol{B_t}\boldsymbol{u_{t-1}} \\ \overline{\boldsymbol{\Sigma}}_{\boldsymbol{t}} = \boldsymbol{A_t}\boldsymbol{\Sigma_{t-1}}\boldsymbol{A_t^T} + \boldsymbol{R_t} \end{gathered} \tag{9}$$

$$\begin{gathered} \boldsymbol{K_t} = \overline{\boldsymbol{\Sigma}}_{\boldsymbol{t}}\boldsymbol{C_t^T}\left(\boldsymbol{C_t}\overline{\boldsymbol{\Sigma}}_{\boldsymbol{t}}\boldsymbol{C_t^T} + \boldsymbol{Q_t}\right)^{-1} \\ \boldsymbol{\mu_t} = \overline{\boldsymbol{\mu_t}} + \boldsymbol{K_t}(\boldsymbol{z_t} - \boldsymbol{C_t}\overline{\boldsymbol{\mu_t}}) \\ \boldsymbol{\Sigma_t} = (\boldsymbol{I} - \boldsymbol{K_t}\,\boldsymbol{C_t})\overline{\boldsymbol{\Sigma}}_{\boldsymbol{t}} \end{gathered} \tag{10}$$

Similar to Equations 9 and 10, in EKF, *prediction update* step is represented in Equation 11, and *measurement update* step is shown in Equation 12. $\boldsymbol{P}$ is the state covariance matrix, $\boldsymbol{Q}$ is the covariance matrix which characterizes the input noise, and, $\boldsymbol{R}$ is the measurement noise covariance matrix for the outputs. $\boldsymbol{\Phi}$ represents the state transition matrix and $\boldsymbol{\Psi}$ is its integral. For linearization, Jacobian matrices are defined in Equation 14. In this study, Jacobian matrices are found by taking analytical derivatives for each state equation in order to eliminate errors as much as possible; however, as expected, it is very time consuming to derive the formulas, and it is recommended to use numerical derivation for complex mathematical models.

$$\begin{gathered} \boldsymbol{x(k+1)} = \boldsymbol{x(k)} + \int_{\boldsymbol{t_k}}^{\boldsymbol{t_{k+1}}} \boldsymbol{f}\big(\boldsymbol{x(t)}, \boldsymbol{u_m(k)}\big)\boldsymbol{dt} \\ \boldsymbol{P(k+1)} = \boldsymbol{\Phi(k+1)P(k)\Phi^T(k+1)} + \boldsymbol{\Psi(k+1)B(k)Q(k)B^T(k)\Psi^T(k+1)} \end{gathered} \tag{11}$$

$$\begin{gathered} \boldsymbol{K(k)} = \boldsymbol{P(k)C^T(k)}[\boldsymbol{C(k)P(k)C(k)} + \boldsymbol{R(k)}]^{-1} \\ \boldsymbol{x(k)} = \boldsymbol{x(k)} + \boldsymbol{K(k)}[\boldsymbol{z(k)} - \boldsymbol{g(x(k))}] \\ \boldsymbol{P(k)} = [\boldsymbol{I} - \boldsymbol{K(k)C(k)}]\boldsymbol{P(k)} \end{gathered} \tag{12}$$

$$\boldsymbol{\Phi(k) = e^{A(k)\Delta t}}$$
$$\boldsymbol{\Psi(k) = \frac{\Phi(k) - I}{A(k)}} \tag{13}$$

$$\boldsymbol{A(k) = \frac{\partial f(x(k),u(k))}{\partial x(k)}} \qquad \boldsymbol{B(k) = \frac{\partial f(x(k),u(k))}{\partial u(k)}} \qquad \boldsymbol{C(k) = \frac{\partial g(x(k))}{\partial x(k)}} \tag{14}$$

In addition, it is worth to mention that while calculations of state transition matrix and its integral in Equation 11, exponential and division operations with the state matrix caused numerical instabilities and errors. Therefore, it is decided to neglect high order terms in the Taylor Series Expansion of state transition matrix as in the reference [Gelb, 2010]. Hence, the state covariance matrix calculation is approximated as;

$$\boldsymbol{P = (I + A\Delta t)P(I + A\Delta t)^T + BQB^T\Delta t} \tag{15}$$

Results & Discussion

Firstly, MR azimuth and MR speed estimations are performed by using KF. TAC and ECU sensors are used for azimuth and speed measurements, respectively. In this case, the input to the linear model is the acceleration of MR which is not measured and remains as unknown; however, since the MR speed is expected as constant throughout the test, there should not be any acceleration too. Therefore, zero input is fed into the model with a sufficiently large process noise covariance matrix. The measured and the estimated values for MR azimuth and the MR speed are shown in Figure 1. Note that the azimuth values are plotted as de-trended due to visual aims. It is clearly seen that although artificial differences are applied to initial values, the states quickly converge to measured values and follow the signals smoothly.

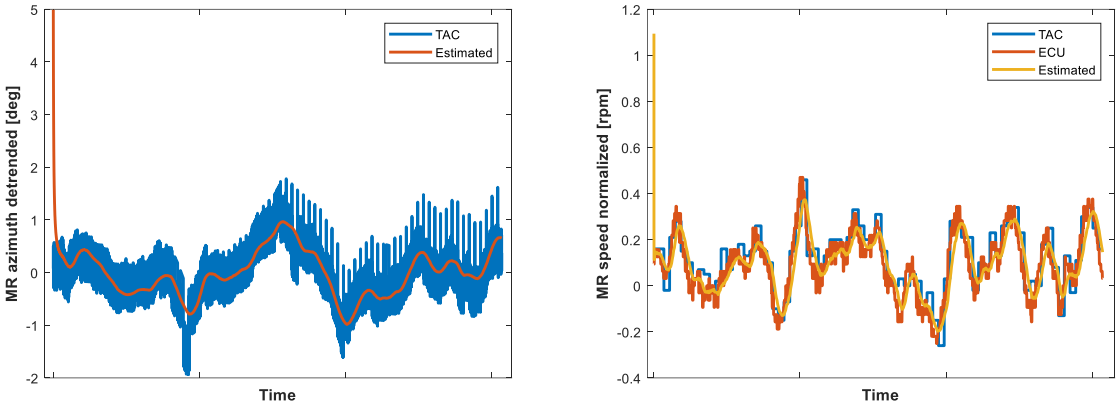

Figure 1: MR azimuth estimation (on the left) and MR speed estimation (on the right) with KF

Secondly, the input is estimation is performed by introducing the inputs as another states. In this case, the input is chosen as the MR speed and; therefore, after the estimation, it can be compared with the measured values. Hence, the mathematical model consists of only one equation and state matrix has size of 1. It is emphasized that MR speed measurements are not used in this procedure, but only MR azimuth measurement data is used. The estimated MR speed and the measurements from different sensors are shown in Figure 2. At the start, a small difference is applied here too. The results show that the input of the system can be estimated. In this case, it is noticed that the estimation quality is very dependent on the measurement noise covariance matrix. If the variance is large in order to be conservative, the estimation cannot capture the local fluctuations. The best value for the noise covariance matrix

is found by trial and error. In addition, it can be seen that there are sudden movements in the estimated signal. This is due to low resolution of TAC sensor. Abrupt changes in the azimuth data make its derivative unrealistic, and hence, speed estimate tries to fit that derivative value. In order to eliminate this phenomena, a smoothing should be applied to the azimuth data as a preprocess. However, it is not preferred at this stage because estimated MR speed value is not used in a further study.

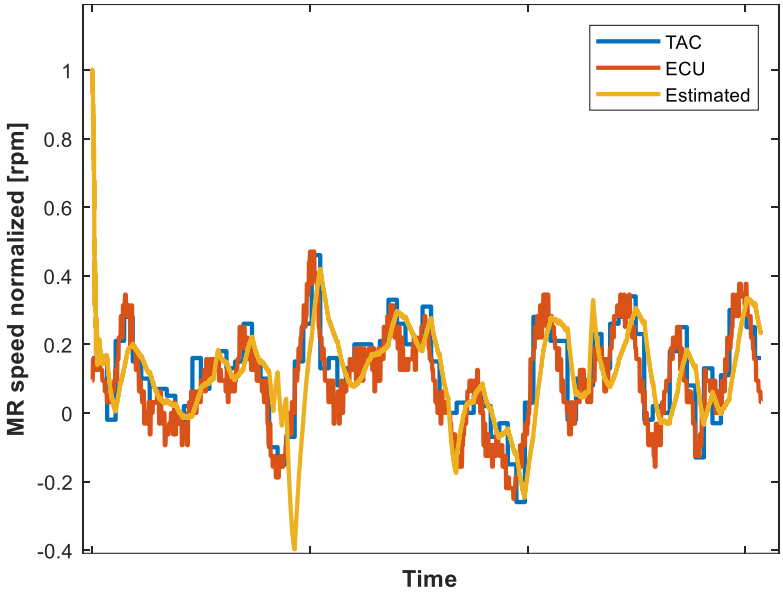

Figure 2: MR speed (input) estimation with KF

Finally, the body and the wind states are estimated by using EKF. Since the nonlinearities are wanted to be included in the model for further studies, EKF method is selected. The measurement data is obtained from AHRS, and therefore, the accuracy of measured signals are very high. In this case, body accelerations and body rates are measured and those values are fed into the model. The results for body velocity $\boldsymbol{w}$ and body pitch angle $\boldsymbol{\theta}$ are demonstrated in Figure 3 and Figure 4, respectively. It is noted that 3σ bounds are drawn for the estimated value and it indicates that the true value is in that region with 99.7% probability. At this point, it should be underlined that since this study is conducted for real flight test data, the true value is unknown. The results show that although there is an initial difference, 5 m/s for $\boldsymbol{w}$ and 5 degrees for $\boldsymbol{\theta}$, the estimation values converge immediately and follow the measured signals. It is observed that there are regions at which the variances increase meaning that the uncertainty is relatively high. More figures showing the body state estimations are given in the Appendix part.

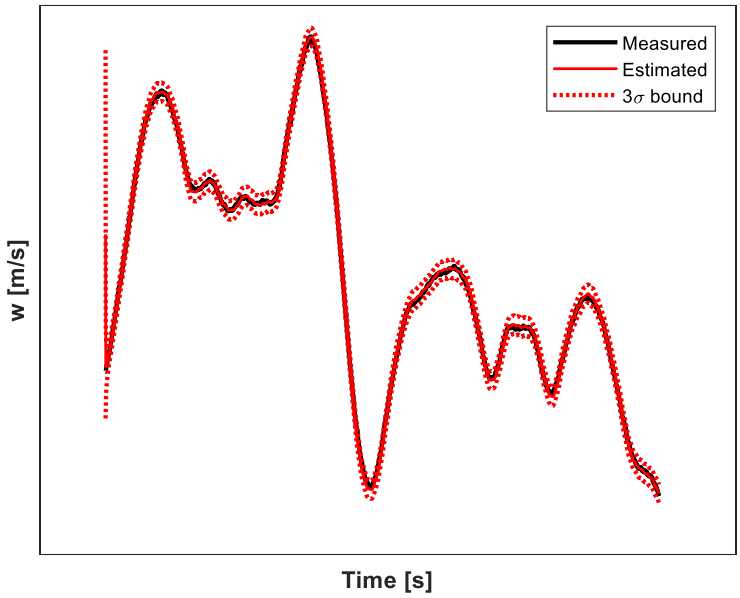

Figure 3: The measured and EKF estimated values for body velocity w

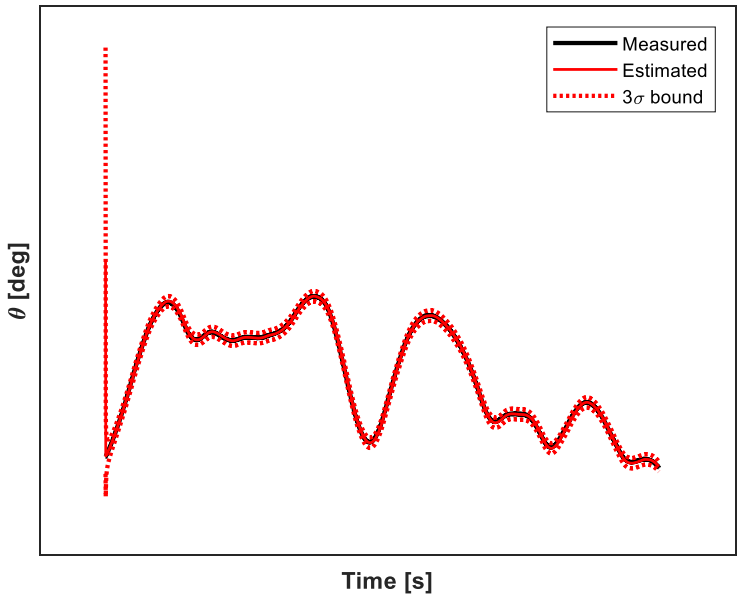

Figure 4: The measured and EKF estimated values for body pitch angle θ

In Figure 3 and Figure 4, it is very hard to capture the convergence and to differ the measured and estimated signals because AHRS accuracy is very high. Therefore, a close look is shown in Figure 5 on the left. EKF enhances the 2σ bound from 1 degree to about 0.1 degree. For comparison, initial difference is increased and measurement noise covariance matrix is increased tenfold on the right plot. Actually, this comparison reveals the power of Kalman filter.

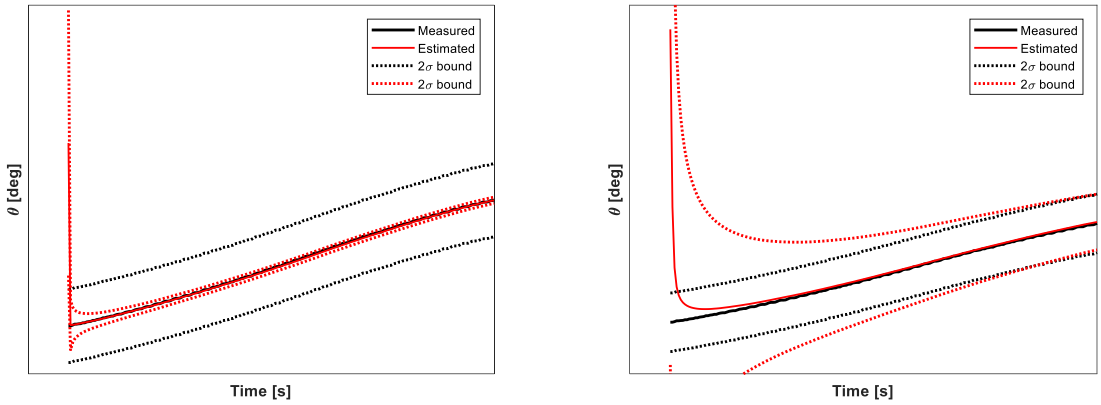

Figure 5: On the left, a close view of the measured and EKF estimated values for body pitch angle θ. On the right, the measured and EKF estimated values for body pitch angle θ for tenfold increased variance

In this case, in addition to body states, wind states are estimated too. Unlike body accelerations and body rates, wind acceleration data is not available; however, it is added into the input vector as zero because the wind speed is expected as nearly constant. In order to estimate the wind speed, some flexibility is required for the wind states, and hence, the wind acceleration variances in the input noise covariance matrix are chosen as larger values compared to others. The wind speed is obtained in body frame and coordinate transformation is applied in order to compare with another measurement data. The results are shown in Figure 6. It should be noted that the measurement data used in EKF comes from Air Data Boom (ADB); however, the drawn measured signals in Figure 6 are obtained from the pitot tube signals which are used in the pilot display. Therefore, pitot tube signals do not reflect rapid fluctuations. In short, comparison for only mean values would make sense.

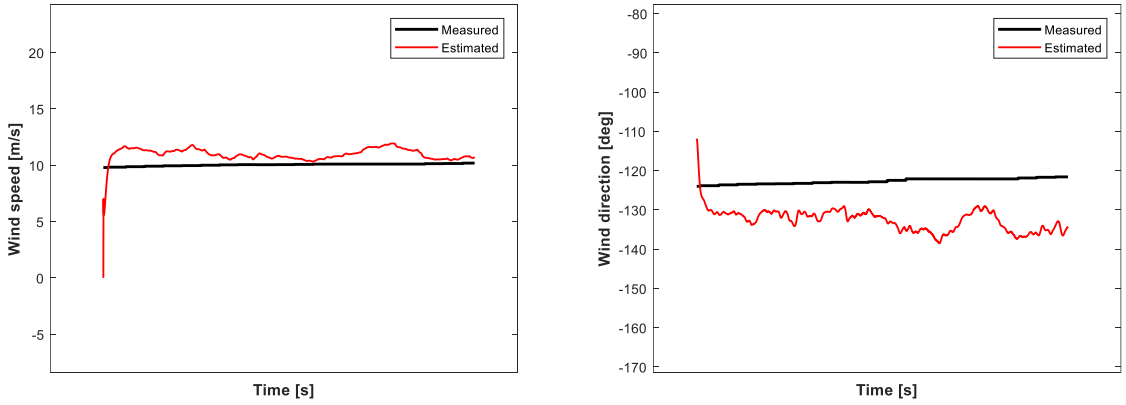

Figure 6: The measured and EKF estimated values for wind speed and wind direction (0 degree points the north and positive direction is clockwise)

Conclusion

In this study, the data consistency check is performed by using the Kalman Filter for T625 helicopter flight test data. First, main rotor azimuth and speed measurement consistency is checked using KF for driveshaft rotational kinematics and dynamics. Driveshaft model input is also estimated in this case. Then, the data compatibility check is performed for the helicopter using EKF for the equations of motion and, in addition, wind speed and direction is estimated. It can be stated that for both models, the states can be well estimated although some states

are not directly measured. It is seen that high accuracy in the measurements positively affects the estimates and a dependable mathematical model increases the accuracy even higher.

Future Work

The study aims to perform a compatibility check for all possible measured states of the T625 helicopter in a flight test. After gaining trust to state model, output model and the implementation of KF and EKF, some important states of main rotor, wind, inflow and empennage can be predicted without any sensor need. At the first stage, the aim is to estimate the wind parameters accurately. In the study, the wind parameters are estimated; however, measurements that are more trustworthy are needed for comparison. Next, the blade flapping and lagging angle estimations can be performed and the study can move towards model validation by estimating MR force & moment.

References

Abreu, José & Oliveira, Roberto & Neto, João. (2020). Rocket tracking impact point prediction using α-β, standard Kalman, extended, Kalman, and unscented Kalman filters: a comparative analysis. Research, Society and Development. 9. 42932022. 10.33448/rsd-v9i3.2022.

Bach, R. E., Jr., "*State Estimation Applications in Aircraft Flight-Data Analysis:*

A User's Manual for SMACK," NASA RP 1252, March 1991.

Evans, R., Goodwin, G., Feik, R., Martin, C., & Lozano-Leal, R. (1985). Aircraft flight data compatibility checking using maximum likelihood and extended kalman filter estimation. *IFAC Proceedings Volumes, 18*(5), 487-492. Doi: 10.1016/s1474-6670(17)60607-4

Fletcher, J. W., "Obtaining Consistent Model of Helicopter Flight-Data Measurement Errors Using Kinematic-Compatibility and State-Reconstruction Methods," *American Helicopter Society Annual Forum*, May 1990.

Gelb, A. (2010). Applied optimal estimation. MIT Press.

Jategaonkar, R. (2006). *Flight Vehicle System Identification: A Time-Domain Methodology.* Reston, VA: American Institude of Aeronautics and Astronautics.

Klein, V., and Schiess, J. R., "*Compatibility Check of Measured Aircraft Responses Using Kinematic Equations and Extended Kalman Filter*," NASA TN D-8514, Aug. 1977.

Nasir, Nabil & Zakaria, Muhammad & Razali, Saifudin & Abu, Mohd. (2017). Autonomous mobile robot localization using Kalman filter. MATEC Web of Conferences. 90. 01069. 10.1051/matecconf/20179001069.

Schiess, J. & Roland, V.. (1975). Kalman filter estimation of human pilot-model parameters.

Soken, Halil & Sakai, Shin-ichiro. (2015). Adaptive Tuning of the Unscented Kalman Filter for Satellite Attitude Estimation. Journal of Aerospace Engineering. 28. 10.1061/(ASCE)AS.1943-5525.0000412.

Tang, Y.M. & Borrie, J.A.. (1984). Missile Guidance Based On Kalman Filter Estimation Of Target Maneuver. Aerospace and Electronic Systems, IEEE Transactions on. AES-20. 736 - 741. 10.1109/TAES.1984.310456.

Thrun, S., Burgard, W., & Fox, D. (2005). *Probabilistic Robotics (Intelligent Robotics and Autonomous Agents series)* (1st ed.). The MIT Press.

Tischler, M. B., & Remplr, R. K. (2006). *Aircraft and Rotorcraft System Identification (AIAA Education Series)* (2nd ed.). American Institude of Aeronautics and Astronautics.

Verhaegen, M., & Verdult, V. (2012). *Filtering and system identification: A least squares approach*. Cambridge University Press.

Wingrove, R. C., “Applications of a Technique for Estimating Aircraft States from Recorded Flight Test Data,” AIAA, Paper 72-965, Sept. 1972.

Xiong, Rong & Chu, Jian. (2006). An Approach to Estimate Robot Pose under Uncertainty. 10.1109/WCICA.2006.1713721.

Appendix

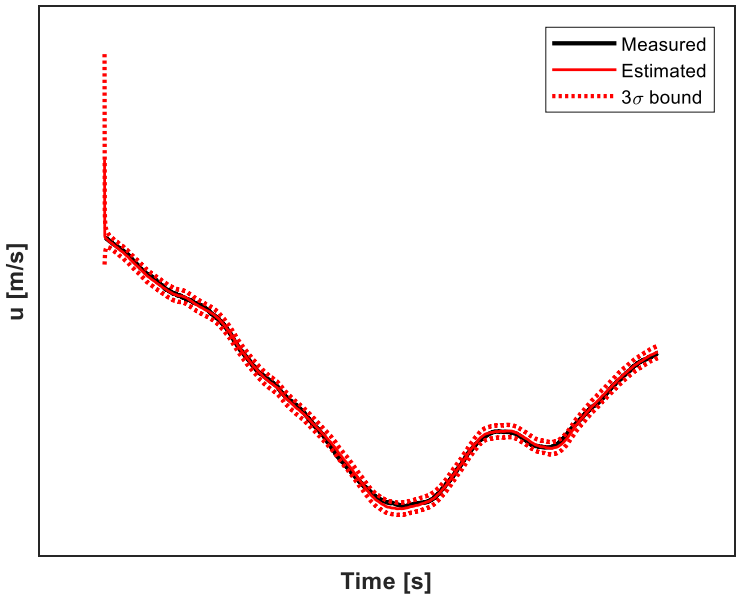

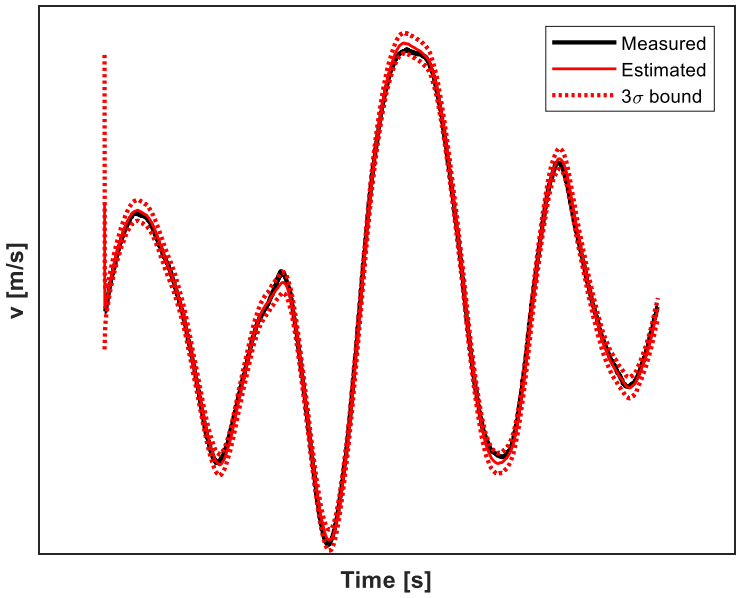

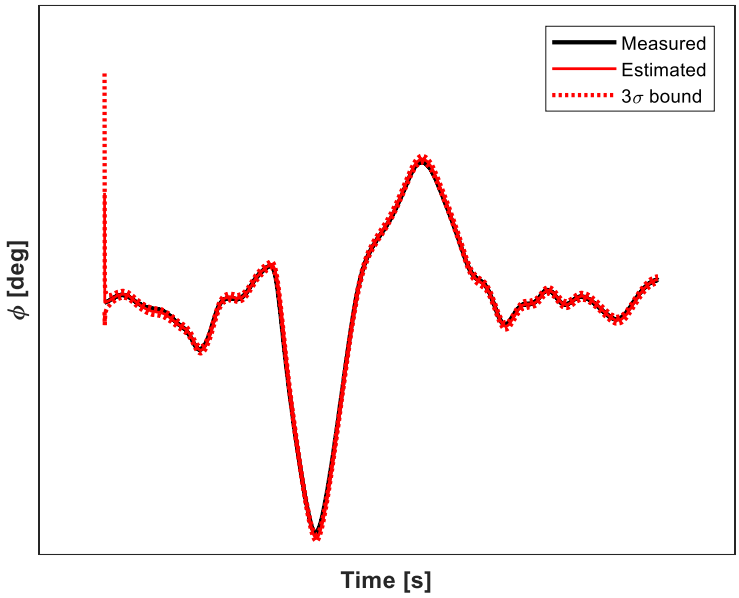
Measured
Estimated
3σ bound
ϕ [deg]
Time [s]

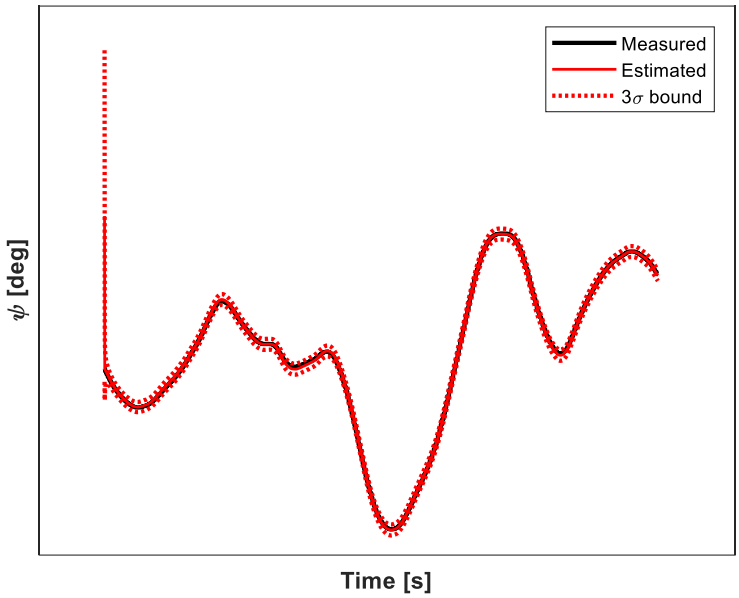
Measured
Estimated
3σ bound
ψ [deg]
Time [s]